On the role of enthalpic and entropic contributions to the conformational free energy landscape of MIL-101(Cr) secondary building units

Loukas Kollias[1], David C. Cantu[2], Vassiliki-Alexandra Glezakou[3*], Roger Rousseau[3], Matteo Salvalaglio[1*]
[1]*Thomas Young Centre and Department of Chemical Engineering, University College London, London WC1E 7JE, United Kingdom;*
[2]*Chemical and Materials Engineering Department, University of Nevada, Reno, Reno, NV, 89557, United States;*
[3]*Basic and Applied Molecular Foundations, Pacific Northwest National Laboratory, Richland, WA, 99352 United States*
KEYWORDS: Molecular Dynamics, Metal-Organic Frameworks, Entropy

ABSTRACT: The thermo-structural behavior of metal-organic framework (MOF) precursors is responsible for regulating the introduction of defects in MOF structures during synthesis. In this paper, factors affecting the flexibility of MIL-101(Cr) half-secondary building units (half-SBUs) are evaluated in solution using enhanced sampling methods. In particular, entropic and enthalpic contributions to the conformational free energy landscape of isolated MIL-101(Cr) half-SBUs are calculated in water, in the presence and absence of ionic species (Na^+ and F^-), and in N, N-dimethylformamide (DMF). This analysis leads to the observation that the interplay between enthalpy and entropy determines the most probable conformational state for half-SBUs. Furthermore, the role of enthalpy and entropy in the conformational rearrangement of an SBU is investigated in water, noting that entropic contributions are essential to stabilize configurations that depart from those coherent with the MIL-101(Cr) crystal structure. This analysis highlights the importance of explicitly considering entropic effects on the configurational ensembles of MOF building units and highlights the significant impact they have on the relative stability of crystal-like and non-crystal-like conformers.

INTRODUCTION

Elucidating the nature of enthalpic and entropic contributions is of significant importance for several processes in organometallic chemistry[1-3] such as in peptide – metal nanoparticle[3] systems. Surface stability[4], solute aggregation[5], supramolecular encapsulation[6] and preferential adsorption of compounds[7] are a few examples of entropically driven processes. Also, entropy – enthalpy compensation phenomena in small solvated solutes, especially proteins, are of particular scientific interest to thoroughly understand the functioning mechanisms of molecules in solution[1, 6, 8-12].

Flexibility is associated with configurational entropy and this can determine the structure and functionality of a molecule[13]. Metal-organic frameworks (MOFs) are built out of flexible building units. A rich conformational ensemble unveiled during the association-dissociation of secondary building units (SBUs)[14] highlights the importance of understanding the origin of the contributions to the free energy landscape of half-SBUs. We recently proposed that the early stages of MOF nucleation are defined by the assembly of half-SBUs into SBU-containing MOF precursors[14-15]. However, the drivers of SBU and half-SBU flexibility are yet to be understood from a thermodynamics perspective.

For instance, the propensity of healing defects in the crystal lattice can be linked with the population of different isomers as well as the guest molecules present during the nucleation stages[14]. Therefore, it is essential to trace back to the origins of this selectivity and understand how different isomers function in the presence of guest molecules. A regulation of the population of defects, which is highly desirable in MOF synthesis[16-19], can thus be rationalized and achieved.

Assessing the entropic and enthalpic profiles of half-SBUs can prove essential to manipulate the thermostructural behavior of MOFs, which are considerably less thermally stable than zeolites[20]. Nevertheless, MOFs are significantly more porous. Therefore, analyzing their thermostructural behavior can provide insights into improving their robustness for a plethora of applications. Mechanical flexibility[21] and thermal expansion[22] of MOFs have been investigated in previous works. Nevertheless, the enthalpic and entropic drivers to the assembly free energy of building units were not assessed. Computational[20, 23-24] and experimental[25] studies on enthalpic and entropic contributions to the adsorption free energy have been frequently carried out for MOFs[20, 23, 25] and metal clusters[24] with a focus on applications. In the field of MOF synthesis, there is a growing effort to improve the mechanical stability of MOFs by taking advantage of novel techniques[26-28]. However, understanding of the entropic and enthalpic contributions to the free energy of half-SBU flexibility is an underexplored area, which has the potential to devise strategies on improving MOFs' intrinsic characteristics during synthesis.

In this work, we evaluate entropic–enthalpic contributions to the free energy profile associated with structural fluctuations in half-SBUs and SBUs. It should be noted that nucleation follows the formation of half – SBUs[15]. These have been discussed extensively in previous works[14-15]. Succinctly, half – SBUs MLA and MLB are stereo isomers and MLC is a structural isomer of both MLA and MLB[14]. The SBU resulting from two MLA half – SBUs (AA SBU) is the one that dominated the equilibrium distribution of all other SBUs[14]. Furthermore, AA contributed to the fraction of crystal – like SBUs more than any other isomer[14].

This analysis allows for an evaluation of the conformational freedom that different molecules experience in solution. This, in turn, leads to a detailed understanding of their flexibility and provides further insight into the nature of the configurational ensembles likely to be visited during self-assembly and nucleation. In addition to this analysis, we calculate the inertia tensor for each isomer, of the MIL-101(Cr) half-SBU[14-15], as well as its solvation behavior in different environments. These complementary pieces of information provide detailed insight into the molecular behavior of MOF building units which drives self-assembly and self-healing during synthesis.

METHODS

Simulation setup

Molecular dynamics (MD) simulations were performed in explicit solvent. The leapfrog integrator was used to propagate dynamics of the system with a time step of 2 fs. The LINCS[29] algorithm preserved the distances of bonds involving hydrogen atoms. The cutoff for non-bonded interactions is 10 Å. Long range electrostatics were treated using the Particle-Mesh Ewald (PME)[30] scheme. The velocity rescaling thermostat[31] and the Berendsen barostat[32] preserved the temperature and pressure at 298 K and 1 bar respectively. To investigate higher temperature conditions, additional NVT simulations are performed at 493 K, consistent with MIL-101(Cr) experimental synthesis[33]. The system is simulated under a high pressure as in an autoclave employed during synthesis[33]. In more detail, the system of isolated half-SBUs (MLA, MLB and MLC)[14-15] in solution, which consists of 6,500 atoms, was simulated in a cubic box of edge 40 Å with periodic boundary conditions in three dimensions. The system of an SBU in solution has 12,000 atoms in a cubic cell with edge equal to 50 Å. Solvent has been treated explicitly with the TIP3P model[34] and ions with the OPLS-AA force field[35]. The force field for the half-SBU species is discussed in detail in a previous work[14-15]. Simulations were carried out using GROMACS 2018[36] and PLUMED 2.5[37]. Chemical structures were visualized using VMD[38]. All the data and PLUMED input files required to reproduce the results reported in this paper are available on PLUMED-NEST (www.plumed-nest.org), the public repository of the PLUMED consortium[39], as plumID:19.073.

Well-tempered metadynamics (WTmetaD)[40] is employed to enhance sampling and construct free energy surfaces along chemically intuitive collective coordinates. In this context, we construct a bias potential as a function of the mass-weighted radius of gyration (R_{gyr}) to assess the flexibility of the MIL-101(Cr) half-SBUs[15]. The radius of gyration has been chosen as a low dimensional descriptor of the conformational state of half-SBUs. In particular we report the value of R_{gyr} for each unit in all our plots.

Gaussians of width 0.1 Å and initial height 0.5975 kcal mol^{-1} were deposited every 1 ps with a bias factor of 10 in absence of ions, and a bias factor of 50 in presence of ions. The total simulation time in water in absence and presence of ions (0.25M), and DMF was 0.5 μs.

Furthermore, a simulation studying the rearrangement of an AA SBU in solution was performed through biasing the coordination numbers greater than 0.5 with a coordination sphere of radius 2.5 Å, and the total potential energy of the system for 1.5 μs at 298 K and 1.0 μs at 493 K. Gaussians of width 0.01 and 47.8 kcal mol^{-1} for coordination number and potential energy were deposited every 1 ps with initial height and bias factor equal to 0.598 kcal mol^{-1} and 100 respectively. A rational switching function[37] with parameters $(d_0 = 0, n = 2, m = 4)$ was used in order to calculate the set of coordination numbers. At last, a harmonic restraining potential (V_r) acted on the lowest component of the set of all distances between any chromium and any terminal carboxylic carbon atoms. The potential, characterized by a force constant of 35.85 kcal mol^{-1} was active when the minimum distance exceeded 3.5 Å. Finally, we have calculated errors on the energy profiles due to sampling following a block analysis. A detailed description is available in the SI, Section VII.

Enthalpic and entropic contributions to the conformational free energy landscape.

As a result of WTmetaD calculations, a free energy surface is the direct output, as a projection of the free energy of the system G in the space of collective variables, denoted with $\boldsymbol{s}$[40]. The Gibbs free energy can be expressed as the sum of its enthalpic and entropic contributions, i.e. $\Delta \mathrm{G}(\mathbf{s}) = \Delta \mathrm{H}(\mathbf{s}) - \mathrm{T} \cdot \Delta \mathrm{S}(\mathbf{s})$, where $\mathrm{G}(\mathbf{s})$ is the free energy, $\mathrm{H}(\mathbf{s})$ the enthalpy, and $\mathrm{S}(\mathbf{s})$ the entropy, and Δ represents the difference with respect to an arbitrarily chosen reference state in $\mathbf{s}$[41].

To systematically decompose the free energy surface $\Delta \mathrm{G}(\mathbf{s})$ we employ the method discussed in Ref. [41], which is based on mapping the ensemble average of the enthalpic component of the free energy in $\mathbf{s}$, and then obtaining the entropic contribution to free energy by difference.

In the case of conformational transitions in solution, associated to negligible variations in the excluded volume, the $P\Delta \mathrm{V}(\mathbf{s})$ contribution to enthalpy (where P is the pressure and $\mathrm{V}(\mathbf{s})$ the volume mapped in CV space) is constant. Hence $\Delta \mathrm{H}(\mathbf{s})$ reduces to the internal energy $\Delta \mathrm{U}(\mathbf{s})$. Furthermore, at constant T, the kinetic energy does not depend on $\mathbf{s}$, and therefore the internal energy contribution $\Delta \mathrm{U}(\mathbf{s})$ further reduces to the potential energy of the system $\Delta E_P(\mathbf{s})$[41].

Since in this work we are analyzing conformational transitions in half-SBUs or SBUs embedded in a solvent, we shall highlight that the potential energy of the system is dominated by the potential energy of the solvent. To limit the statistical uncertainty in the decomposition of the free energy surface $\Delta \mathrm{G}(\mathbf{s})$, we shall therefore further decompose the contributions to $\Delta E_P(\mathbf{s})$ as follows:

$$\Delta E_P(\mathbf{s}) = \Delta\langle E_P^{solute}\rangle_{\boldsymbol{s}} + \Delta\langle E_P^{solute-solvent}\rangle_{s} + \Delta\langle E_P^{solvent}\rangle_{s} + \Delta\langle E_P^{LR}\rangle_{s} \quad (1)$$

Where adopting the notation introduced by Gimondi et al.[41] $\langle E_P^{solute}\rangle_{\boldsymbol{s}}$, and $\langle E_P^{solvent}\rangle_{\boldsymbol{s}}$ represent ensemble averages of the potential energy of the solute projected in $\boldsymbol{s}$, including all the bonded terms (bond, angles, proper dihedrals and Ryckaert-Bellemans dihedrals[42]) of solute and solvent respectively; plus the non-bonded, short-range terms for solute-solute and solvent-solvent interactions. Long-range interactions, $\langle E_P^{LR}\rangle$, are also accounted for all species.

The term $\langle E_P^{solute-solvent}\rangle_{\boldsymbol{s}}$ accounts instead for the non-bonded, short-range potential energy terms associated to solute-solvent interactions.

We shall note that the term $\langle E_P^{solvent}\rangle_s$ is independent from the conformation of the solute mapped on $\mathbf{s}$, hence $\Delta\langle E_P^{solvent}\rangle_s = 0$.

In order to compute $\Delta\langle E_P^{solute}\rangle_s$ and $\Delta\langle E_P^{solute-solvent}\rangle_s$ as discussed in Gimondi et al.[41], we estimate Boltzmann weights using the method of Tiwary and Parrinello[43].

Solvation shell

In order to investigate the role of the solvation shell on the enthalpy and entropy of rearrangement of half-SBUs, we calculate contributions to the potential energy by changing our convention for the molecules considered in the calculation of the term $\Delta\langle E_P^{solute-solvent}\rangle_s$.

In particular we now explicitly distinguish between solvent molecules found within a certain radius from the solute, constituting the solvation shell interacting with the half-SBUs. By considering solvation shells of increasing size (from 2.5 to 20 Å), and monitoring the convergence of the potential energy contribution $\Delta\langle E_P^{solute-solvent}\rangle_s$ as a function of the solvation shell size, we quantify the impact of the half-SBUs conformational rearrangement on the surrounding solvent environment, and assess solvation shell impact on the conformational entropy.

Effect of ions and solvent

The role of ions and the changes in the free energy and the enthalpy-entropy profiles are investigated. Ions (Na^+, F^-) are added at a concentration of 0.25M, with respect to the simulation box, in order to evaluate half-SBU flexibility in excess of ionic species. We complement the interactions between the solute and the solvent with those between the ionic species and the solute. Furthermore, a different solvent can significantly affect the energetics of conformational transformations in the solute. This is due to entropic and enthalpic contributions being affected by the nature of solvation[6]. To assess this effect on MIL-101(Cr) SBUs, in addition to water we investigate N, N-dimethylformamide (DMF). The OPLS forcefield parameter for DMF were obtained from the *virtualchemistry.org* database[44-45].

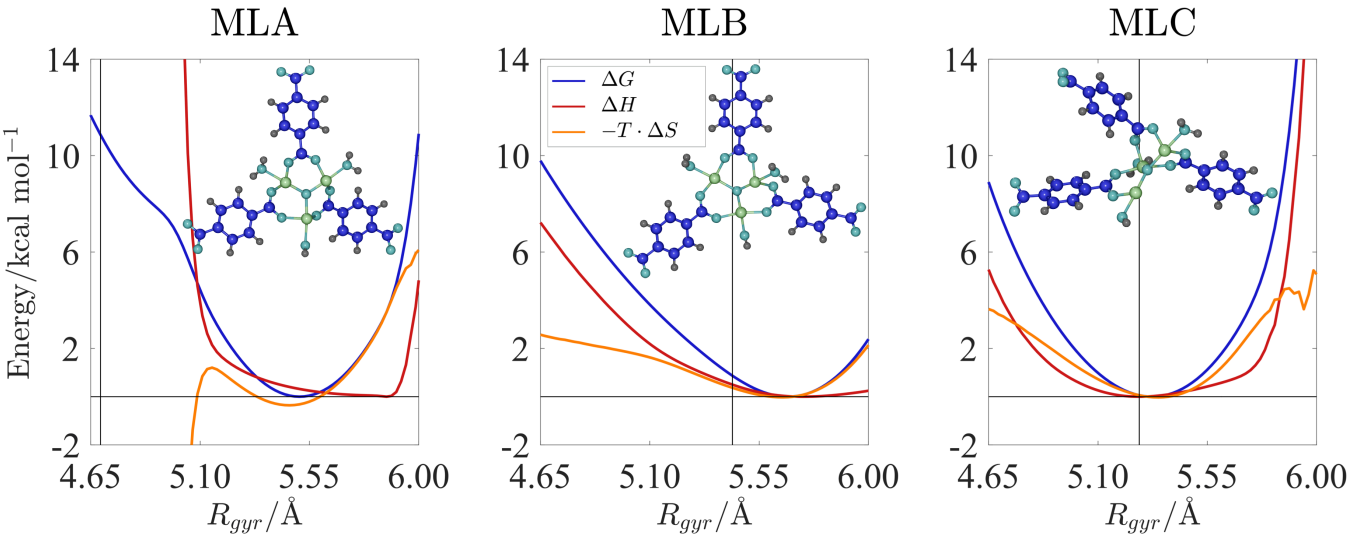

Figure 1. Energy landscape of MLA, MLB and MLC in water at 298 K as a function of R_{gyr}. In blue we report the free energy profile, red: enthalpic contribution, orange: entropic contribution profile. Molecular configurations shown correspond to structures representative of the free energy minima in the respective profiles. Color code: Cr-lime, C-blue, O-cyan and H-gray. A thin horizontal line represents zero on the vertical axis. A thin vertical line corresponds to the average R_{gyr} value of each half-SBU in the crystal.

RESULTS

We investigate the driving forces to the conformational complexity of the half-SBUs of MIL-101(Cr)[33] by exploring the energy profile as a function of R_{gyr}. We carry out this analysis for all three half-SBU isomers identified as key in the early stages of MIL-101(Cr) self-assembly[15], computing the entropic and enthalpic contributions to free energy.

A first observation is that MLA has considerably different free energy and entropy minima, unlike MLB and MLC. In MLA, entropy favors compact configurations (R_{gyr} = 4.77 Å), while enthalpy drives the system to larger values of R_{gyr} (5.87 Å). Higher temperature conditions (493 K) result to a similar free energy minimum compared to 298 K. Enthalpy has a minimum at 5.73 Å that is slightly less than at 298 K. Entropy is dominated by considerably more compact structures than the minimum at 298 K (R_{gyr} = 4.19 Å). The profiles at 493 K are available in the SI, section V.

MLB presents similar values of R_{gyr} for the strongest enthalpic (R_{gyr} = 5.73 Å) and entropic contributions (R_{gyr} = 5.65 Å) to the free energy, corresponding to the largest value of R_{gyr} among the three half-SBUs, at 298 K. MLC presents the minimum enthalpic contribution at a low value of R_{gyr} (5.23 Å); hence rendering more compact configurations enthalpically favored. The entropic contribution has a minimum at 5.37 Å at 298 K. Another straightforward observation is that the minima for the enthalpic and entropic contributions correspond to similar values for R_{gyr} as in MLB, while for MLA the respective R_{gyr} values differ by more than 1 Å.

To summarize the analysis of the energy landscape for half-SBUs in water, the free energy of MLA is dominated by

strongly contrasting enthalpic and entropic effects. Enthalpy favors "open" structures with stretched arms, while entropy favors more compact configurations. In MLB and MLC, enthalpy and entropy contribute in a similar manner to the free energy profile, with their minima exhibiting close values of R_{gyr}. We note that the average values (the standard deviation is provided in brackets) of R_{gyr} in the crystal are 4.69 (0.16) Å for MLA, 5.44 (0.17) Å for MLB and 5.27 (0.13) Å for MLC. Therefore, entropy is the driver to the structures in the crystal for MLA and MLB. More elaborately, R_{gyr} values corresponding to the minimum in the entropic contribution are closer to the average value in the crystal than those dominating the enthalpic contribution. In contrast, enthalpy is dominated by values of R_{gyr} closer to the ones in the crystal, than values corresponding to the minimum entropic contribution, only for MLC. The resulting energy profiles are reported in Figure 1.

Effect of solvation shell

The effect of the solvation shell on the entropic – enthalpic contribution profiles is investigated. Our motivation stems from the need of assessing the interplay between entropy and enthalpy in relation to solvation. For instance, strong enthalpic interactions between the solute and the solvent molecules, within a solvation shell, can induce significant changes in the entropy of these molecules against those far away from the solute[9]. Recently, Schauperl et al.[46] showed that the water model choice can only result in minor differences in the entropy and enthalpy of solvation.

We consider six solvation shell sizes: 2.5, 5, 7.5, 10, 15 and 20 Å. We note that entropy/enthalpy breakdown qualitatively converges for shell sizes larger than 5 Å. Calculating the differences in the enthalpy contribution at different shell sizes we conclude that a solvation shell of 7.5 Å is sufficient to capture solute-solvent interactions. For instance, accounting for a solvation shell of size 7.5 Å produces a maximum difference with respect to the enthalpy profile obtained including all the solvent molecules of the order of k_BT. Such a difference becomes negligible for solvation shell sizes larger than 10 Å, indicating that solute reorganization extends to solvent molecules within this distance. We note that the free energy profile is inherently associated with the configurational space of the entire simulation box, and it is not affected by changes in the size of the solvation shell.

An analogous analysis has been carried out for MLA in aqueous solution, in the presence of ions. Very similar trends are observed as in pure water; hence the solute-solvent interactions are fully captured within a solvation shell of size 7.5-10Å.

The enthalpy and entropy profiles computed as a function of solvation shell size are reported in the Supporting Information (SI), section IV.

In order to understand the effect of solvation on the enthalpic and entropic contributions to the free energy profiles, the radial distribution functions are calculated between the central oxygen of the metal center of each half-SBU ($O_{u,\,MLA}$) and a characteristic atom of each solvent (the oxygen for water and the nitrogen for DMF). Radial distribution functions are reported in SI, section II. In water, the first solvation shell is located 3 Å away from the central oxygen of MLA, in absence and presence of ions, and it contains 3 solvent molecules. The second solvation shell displays a bimodal structure, with the first peak located at 5.2 Å. At 5.7 Å, water displays a second peak in the second solvation shell, while in the presence of ions the second solvation shell is represented by a monomodal peak centered at 5.7 Å. The third solvation shell in water is located between 7.5-8 Å in water, both in presence and absence of counterions. This analysis highlights that the impact on the energetics of the system, induced by the conformational rearrangement of MLA extend up to the fourth coordination shell, involving up to 46 water molecules. Small discrepancies between the radial distribution functions in pure water and in water with ions are expected due to the presence of F^- that perturbs the hydrogen bond network of water[47].

In DMF, the first solvation shell is centered around 5.2 Å with the second solvation shell located at 8 Å. This indicates that in DMF the solute-solvent interplay in the definition of the enthalpic and entropic contributions to the conformational free energy landscape only extends up to the second solvation shell, involving approximately 11 molecules.

Addition of ions

The addition of ions (0.25M) can significantly alter the energetics of the system due to their strong interactions with partially charged atoms of the half-SBU. We analyze contributions to the MLA free energy profile as this presents the strongest electrostatic interactions. The introduction of ionic species results in additional electrostatic and van der Waals contributions to the potential energy with a net effect in favor of electrostatics as the total potential energy is shifted to more negative values compared with the simulations in absence of ions. The free energy profile is considerably less steep than in absence of ions; hence there is a much larger number of configurations which supply similar entropic contributions to the free energy. Furthermore, in presence of ions the free energy is dominated by enthalpy which tends to favor slightly more compact configurations than those corresponding to the free energy minimum.

Significant contributions to the potential energy stem from electrostatic interactions between fluoride anions and chromium atoms of the half-SBU metal center which restrict free movement of the linkers. This highlights that ions entropically alter the energy landscape of the half-SBU flexibility by increasing the set of accessible configurations at a certain value of R_{gyr}; hence increasing the level of degeneracy in the space of R_{gyr}. The latter results in a much wider free energy well compared to the corresponding profiles in pure water.

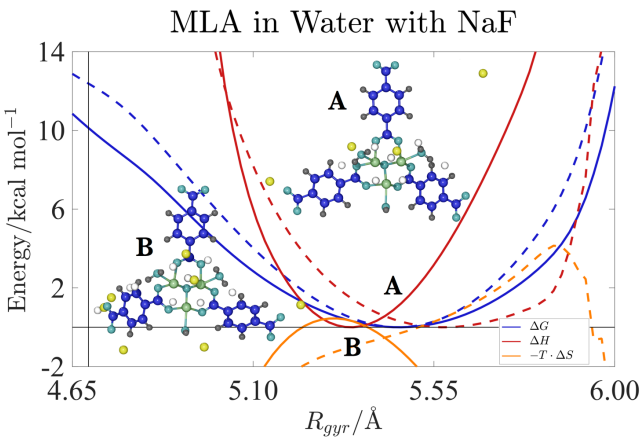

Figure 2. Energy landscape of MLA in water at 298 K (solid lines) and 493 K (dashed lines) with 0.25M NaF as a function of R_{gyr}. Blue: free energy, red: enthalpic contribution, orange: entropic contribution profile. Structure A corresponds to the free energy minimum and B to the enthalpic contribution minimum. The color code is consistent with Fig. 1. A thin horizontal line represents zero on the vertical axis. A thin vertical line corresponds to the average R_{gyr} value of the MLA half-SBU in the crystal.

The use of a higher temperature (493 K) results to a very similar, but more narrow, free energy profile. Nevertheless, the enthalpic and entropic contributions present appreciable changes. Enthalpy is dominated by more open structures that correspond to larger R_{gyr} values (5.35 Å at 298 K and 5.59 Å at 493 K). Entropy favors even more compact structures than at 298 K as it has a minimum at lower R_{gyr} values (4.65 Å at 298 K and 4.49 Å at 493 K). Therefore, the increase of temperature results to highly contrasting enthalpic and entropic contributions in contrast with free energy.

The resulting energy profiles for MLA are available in Figure 2.

Furthermore, the energy profiles for MLB and MLC in water with ions are calculated on the space of R_{gyr}. In MLB, entropy is affected by the modification of the composition of the system as it favors slightly more compact structures than in pure water. Also, the reference structure for the crystal is dominated by the entropic contribution. MLC presents the enthalpic contribution minimum at R_{gyr} values that are very similar to the ones in the crystal. Energy profiles for MLB, MLC in water in presence of ions are available in the SI, section III.

Effect of solvent

The effect of DMF becomes apparent for MLA when the potential energy is projected on collective variable space. Both enthalpy and entropy profiles are monomodal close to the free energy minimum. Also, both provide similar contributions to free energy, in contrast with water, as it can be seen in Figure 3. Nevertheless, the minimum for the entropic contribution is relevant to the one in water for a value of R_{gyr} less than 4.8 Å, while the enthalpic contribution shows a minimum for values close to 5.47 Å.

In DMF, the free energy minimum is very close to the one obtained in water, but the underlying entropic and enthalpic contributions are considerably different. This means that the configurations associated with low values of R_{gyr}; hence corresponding to more compact structures, do not belong to very high potential energy regions, as in water. In other words, DMF does not favor a plethora of entropically accessible microstates for very compact structures. This bulkier solvent hinders the half-SBU flexibility when in compact form; thus, leading to more rigid configurations at low values of R_{gyr}, in comparison with water. This rigidity can be linked with the study of the more stable forms of SBUs in DMF as discussed in another work[14]. At last, energy profiles for MLB and MLC in DMF are available in the SI, section III.

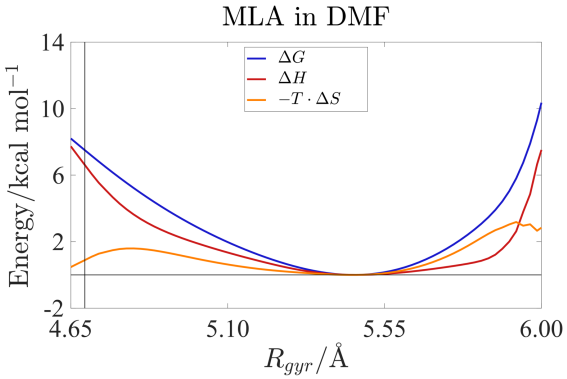

Figure 3. Energy landscape of MLA in DMF at 298 K as a function of R_{gyr}. Blue: free energy, red: enthalpic contribution, orange: entropic contribution profile. A thin horizontal line represents zero on the vertical axis. A thin vertical line corresponds to the average R_{gyr} value of each half-SBU in the crystal.

Isomer symmetry

Another important aspect that can provide significant insight into the conformational flexibility of different isomers is a measure of symmetry along principal axes of inertia. The moments of inertia corresponding to rotational movement around principal axes are calculated and mapped on collective variable space. We calculate the major, middle and minor axes of inertia and the corresponding moments. We observe that the major axis is similar for the three isomers. The middle and minor axes are appreciably different for MLA compared with the other two. Nevertheless, the minor axis for MLA is similar to the middle axis for MLB and MLC.

In water, the moment of inertia corresponding to the major axis has the highest favorable value for MLA and the lowest for MLC. Also, MLA and MLB present a narrower range of values than MLC where the moment of inertia has a very wide distribution. The moment of inertia corresponding to the middle axis has the lowest favorable value for MLA and the highest for MLC. Again, MLA and MLB present a narrower range when compared with MLC. The moment of inertia corresponding to the minor axis presents a narrow distribution and the lowest favorable value for MLC. For MLB, the opposite occurs as it has the highest favorable value and a wide distribution. In addition to water, we assess the probability density of moments of inertia in DMF. Moments that correspond to the major and middle axes show very similar densities when compared with water, while rotation around the minor axis renders the total moment of inertia for MLA lower than in water and closer to MLC; hence it corresponds to a more compact structure that allows the molecule to possess smaller rotational inertia. This analysis offers a

potential explanation to the observation that MLA results in more compact SBUs in DMF[14].

Overall, MLA resists rotational acceleration around its major axis more than MLB and MLC, while it shows lower resistance to rotation around its middle axis when compared with the other two isomers. Also, it has appreciably narrower distributions for its moments of inertia around the major and middle axis than MLB and MLC. MLB has a relatively higher moment of inertia corresponding to its minor axis than MLA and MLC. MLC shows lower resistance to rotational acceleration around its major axis than MLA and MLB. At last, the trend of the total moment of inertia for rotational movement around any axis is very similar to that of R_{gyr} for all isomers. This analysis is available in the SI, section I.

Study of the rearrangement of an SBU

At last, we depart from the assessment of isolated half-SBUs in solution in order to evaluate entropic and enthalpic contributions to the free energy landscape of a half-SBU couple forming an SBU in solution. We start the simulations from a crystal-like SBU and sample the configuration space of different arrangements based on the coordination between terminal carboxylic oxygen atoms of one half-SBU with the chromium atoms at the metal center of the adjacent half-SBU. A value of this collective variable equal to 1.6 corresponds to 2 chromium-oxygen interactions as in the crystal lattice, labelled C for crystal-like. A value of 2.5 is representative of 3 chromium-oxygen interactions, labelled T (for triple chromium-oxygen interaction). At last, a value of this collective variable equal to 3.3 corresponds to 4 chromium-oxygen interactions, labelled Q (indicating a quadruple chromium-oxygen interaction). The energy profiles of the SBU rearrangement show that C is enthalpically dominated, while Q is entropically dominated. Since, Q is the most stable structure from a free energy standpoint, we conclude that the free energy landscape of the rearrangement of an SBU is entropically dominated as seen in Figure 4. Energy profiles are reweighted in order to negate the effect of the bias due to both WTmetaD[40] and V_r. Finally, the entropically dominated Q state is further stabilized at a higher temperature. Therefore, the change of temperature alone cannot lead to the C state dominating free energy. Free energy profiles including enthalpic and entropic contributions at both temperatures and structures characteristic of each state are available in Figure 4.

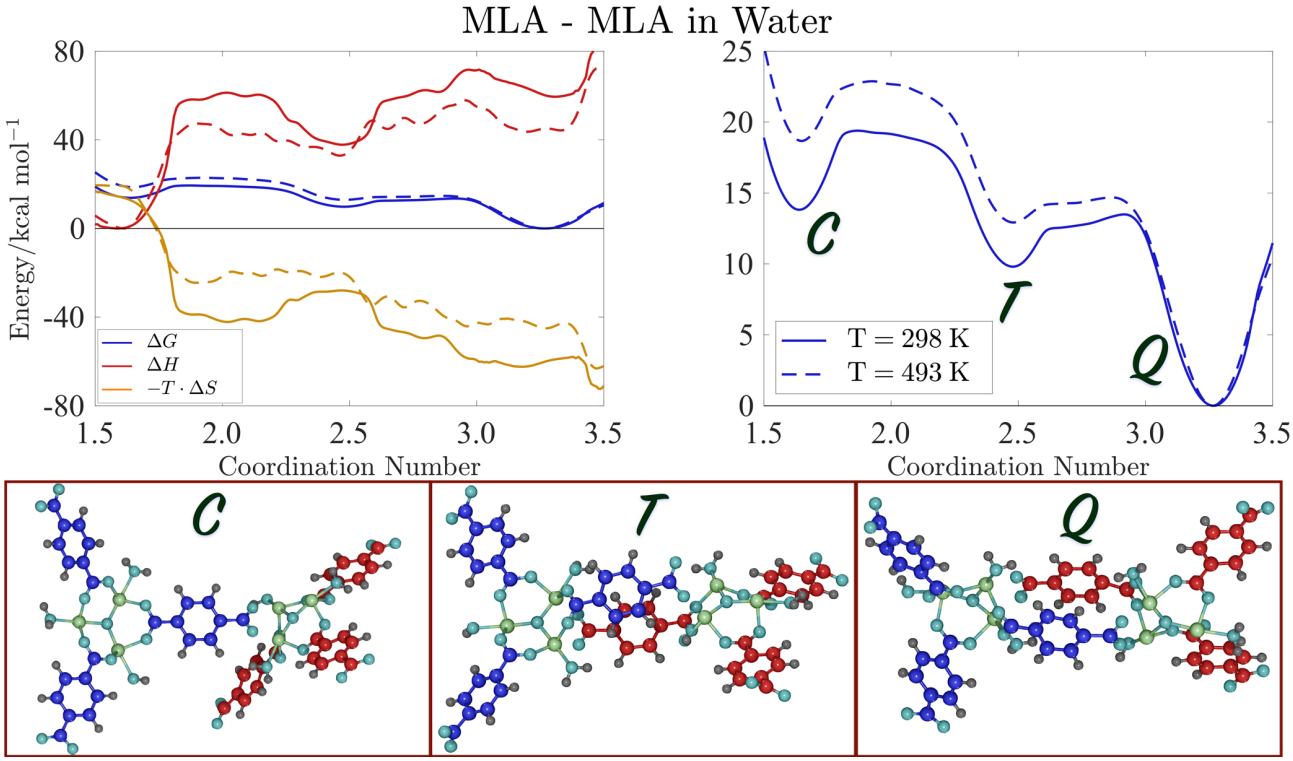

Figure 4. Energy landscape of the rearrangement of an AA SBU in water at 298 K (solid lines) and 493 K (dashed lines) with respect to the coordination number between terminal carboxylic oxygen and adjacent chromium atoms. Left panel: Blue: free energy, red: enthalpic contribution, orange: entropic contribution profile. Right panel: free energy profile in more detail. Configurations corresponding to the C, T and Q states are shown. The color code is consistent with Figure 1, except from carbon atoms that are colored blue for one half-SBU and red for its counterpart. A thin horizontal line represents zero on the vertical axis.

CONCLUSIONS

In this work, we investigate the entropic and enthalpic contributions to the free energy landscape of MOF building units. This enhances our understanding of how the thermo-structural properties of MOF precursors can be fine-tuned. The behavior of MIL-101(Cr) half-SBU isomers[15] is evaluated in different environments, including water, in absence and presence of ions, and DMF, in order to examine the drivers that can render them sources of either crystal-like units or defects[14]. In this effort, we use the mass-weighted radius of gyration (R_{gyr}) as a measure of isomer-specific molecular flexibility.

In water, MLB and MLC present free energy profiles with similar enthalpic and entropic contributions projected on R_{gyr}. The free energy minima correspond to R_{gyr} values between the minima of the entropic and enthalpic contributions. In MLA, the entropic contribution presents a minimum for very low R_{gyr}, while the enthalpic contribution minimum corresponds to a configuration with a large value of R_{gyr}. An increase in temperature results to similar free energy and enthalpy profiles, while entropy favors even more compact structures. A comparison with the R_{gyr} values of the half-SBUs in the crystal shows that MLA and MLB correspond to structures favored by the entropic contribution. MLC half-SBUs in the crystal are closer to structures that dominate the enthalpic contribution.

The presence of ions increases the number of accessible microstates, on R_{gyr} space, sampled during the simulation. Also, the introduction of ions leads to the crystal structure corresponding to R_{gyr} values close to the entropic contribution minimum for MLB and enthalpic contribution minimum for MLC. Therefore, a change in the composition of the system can shift the minima of the enthalpic and entropic contributions to R_{gyr} values similar to those corresponding to half-SBUs in the crystal.

Solvent effects have a considerable impact as the enthalpic and entropic contribution minima for MLA are similar close to the free energy minimum. Furthermore, the compact configuration that corresponds to the entropic contribution minimum in pure water is not as favorable in bulkier solvents such as DMF, as it is in water.

At last, we study the rearrangement of an SBU in water, a process that has been identified as relevant in a previous work[14]. Our analysis shows that the crystal-like configuration of the SBU (C) is enthalpically favored, while SBU configurations displaying multiple concurrent linker-metal center interactions (T, Q) are entropically favored. The Q configurations are further stabilized with an increase in temperature. This allows to identify the configurational entropy contributions as the main driver for the formation of SBUs that depart from the crystal-like configuration and are likely to result in defective materials. Therefore, C can be more probable than Q only with a change in the composition of the system. This can provide a plausible rationale on the use of ions during MOF synthesis[33]. Our findings highlight how static potential energy calculations provide only a partial and perhaps insufficient description of the configurational landscape of MOF building units.

ASSOCIATED CONTENT

Supporting Information

The Supporting Information is available free of charge on the ACS Publications website.

Supplementary information (SI) linked with the main article (PDF)

AUTHOR INFORMATION

Corresponding Author

*vanda.glezakou@pnnl.gov
*m.salvalaglio@ucl.ac.uk

Notes

The authors declare no competing financial interest.

ACKNOWLEDGMENT

The work described in this publication was performed by Pacific Northwest National Laboratory (PNNL), which is operated by Battelle for the United States Department of Energy (DOE) under Contract DE-AC05-76RL0180. V.-A. G. and R. R. acknowledge support from DOE Office of Basic Energy Sciences – Chemical, Geological and Biological Sciences Division. L. K. was partially supported by a Laboratory Directed Research and Development grant for PNNL. D.C.C. acknowledges support from Research and Innovation at the University of Nevada, Reno. The authors acknowledge the use of the UCL Myriad High Throughput Computing Facility (Myriad@UCL), and associated support services, in the completion of this work. We are grateful to the UK Materials and Molecular Modelling Hub for computational resources, which is partially funded by EPSRC (EP/P020194/1). This research used resources of the National Energy Research Scientific Computing Center, a DOE Office of Science of the U.S. Department of Energy under Contract No. DE-SUPPLEMENTARY MATERIAL AC02-05CH11231.

REFERENCES

1. Choudhury, N.; Pettitt, B. M., Enthalpy-entropy contributions to the potential of mean force of nanoscopic hydrophobic solutes. *J Phys Chem B* **2006,** *110* (16), 8459-63.
2. van der Vegt, N. F. A.; van Gunsteren, W. F., Entropic Contributions in Cosolvent Binding to Hydrophobic Solutes in Water. *The Journal of Physical Chemistry B* **2004,** *108* (3), 1056-1064.
3. Tang, Z.; Palafox-Hernandez, J. P.; Law, W.-C.; Hughes, Z. E.; Swihart, M. T.; Prasad, P. N.; Knecht, M. R.; Walsh, T. R., Biomolecular Recognition Principles for Bionanocombinatorics: An Integrated Approach To Elucidate Enthalpic and Entropic Factors. *ACS Nano* **2013,** *7* (11), 9632-9646.
4. Amirjalayer, S.; Tafipolsky, M.; Schmid, R., Surface Termination of the Metal-Organic Framework HKUST-1: A Theoretical Investigation. *The Journal of Physical Chemistry Letters* **2014,** *5* (18), 3206-3210.
5. Mondal, J.; Yethiraj, A., Driving Force for the Association of Amphiphilic Molecules. *The Journal of Physical Chemistry Letters* **2011,** *2* (19), 2391-2395.
6. Leung, D. H.; Bergman, R. G.; Raymond, K. N., Enthalpy−Entropy Compensation Reveals Solvent Reorganization as a Driving Force for Supramolecular Encapsulation in Water. *Journal of the American Chemical Society* **2008,** *130* (9), 2798-2805.
7. Van de Voorde, B.; Boulhout, M.; Vermoortele, F.; Horcajada, P.; Cunha, D.; Lee, J. S.; Chang, J.-S.; Gibson, E.; Daturi, M.; Lavalley, J.-C.; Vimont, A.; Beurroies, I.; De Vos, D. E., N/S-Heterocyclic Contaminant Removal from Fuels by the Mesoporous Metal–Organic Framework MIL-100: The Role of the Metal Ion. *Journal of the American Chemical Society* **2013,** *135* (26), 9849-9856.
8. Eftink, M. R.; Anusiem, A. C.; Biltonen, R. L., Enthalpy-entropy compensation and heat capacity changes for protein-ligand interactions: general thermodynamic models and data for the binding of nucleotides to ribonuclease A. *Biochemistry* **2002,** *22* (16), 3884-3896.

9. Lumry, R.; Rajender, S., Enthalpy-entropy compensation phenomena in water solutions of proteins and small molecules: a ubiquitous property of water. *Biopolymers* **1970,** *9* (10), 1125-227.
10. Mills, E. A.; Plotkin, S. S., Protein Transfer Free Energy Obeys Entropy-Enthalpy Compensation. *The Journal of Physical Chemistry B* **2015,** *119* (44), 14130-14144.
11. Pan, A.; Biswas, T.; Rakshit, A. K.; Moulik, S. P., Enthalpy–Entropy Compensation (EEC) Effect: A Revisit. *The Journal of Physical Chemistry B* **2015,** *119* (52), 15876-15884.
12. Pan, A.; Kar, T.; Rakshit, A. K.; Moulik, S. P., Enthalpy–Entropy Compensation (EEC) Effect: Decisive Role of Free Energy. *The Journal of Physical Chemistry B* **2016,** *120* (40), 10531-10539.
13. Brady, J.; Karplus, M., Configuration entropy of the alanine dipeptide in vacuum and in solution: a molecular dynamics study. *Journal of the American Chemical Society* **1985,** *107* (21), 6103-6105.
14. Kollias, L.; Cantu, D. C.; Tubbs, M. A.; Rousseau, R.; Glezakou, V. A.; Salvalaglio, M., Molecular Level Understanding of the Free Energy Landscape in Early Stages of Metal-Organic Framework Nucleation. *J Am Chem Soc* **2019,** *141* (14), 6073-6081.
15. Cantu, D. C.; McGrail, B. P.; Glezakou, V. A., Formation Mechanism of the Secondary Building Unit in a Chromium Terephthalate Metal-Organic Framework. *Chemistry of Materials* **2014,** *26* (22), 6401-6409.
16. Taddei, M., When defects turn into virtues: The curious case of zirconium-based metal-organic frameworks. *Coordination Chemistry Reviews* **2017,** *343*, 1-24.
17. Howarth, A. J.; Liu, Y.; Li, P.; Li, Z.; Wang, T. C.; Hupp, J. T.; Farha, O. K., Chemical, thermal and mechanical stabilities of metal–organic frameworks. *Nature Reviews Materials* **2016,** *1* (3).
18. Gutov, O. V.; Gonzalez Hevia, M.; Escudero-Adan, E. C.; Shafir, A., Metal-Organic Framework (MOF) Defects under Control: Insights into the Missing Linker Sites and Their Implication in the Reactivity of Zirconium-Based Frameworks. *Inorg Chem* **2015,** *54* (17), 8396-400.
19. Howarth, A. J.; Peters, A. W.; Vermeulen, N. A.; Wang, T. C.; Hupp, J. T.; Farha, O. K., Best Practices for the Synthesis, Activation, and Characterization of Metal–Organic Frameworks. *Chemistry of Materials* **2016,** *29* (1), 26-39.
20. Torres-Knoop, A.; Dubbeldam, D., Exploiting Large-Pore Metal-Organic Frameworks for Separations through Entropic Molecular Mechanisms. *ChemPhysChem* **2015,** *16* (10), 2046-2067.
21. Sarkisov, L.; Martin, R. L.; Haranczyk, M.; Smit, B., On the Flexibility of Metal–Organic Frameworks. *Journal of the American Chemical Society* **2014,** *136* (6), 2228-2231.
22. Balestra, S. R. G.; Bueno-Perez, R.; Hamad, S.; Dubbeldam, D.; Ruiz-Salvador, A. R.; Calero, S., Controlling Thermal Expansion: A Metal–Organic Frameworks Route. *Chemistry of Materials* **2016,** *28* (22), 8296-8304.
23. Torres-Knoop, A.; Poursaeidesfahani, A.; Vlugt, T. J. H.; Dubbeldam, D., Behavior of the Enthalpy of Adsorption in Nanoporous Materials Close to Saturation Conditions. *Journal of Chemical Theory and Computation* **2017,** *13* (7), 3326-3339.
24. Gomez, D. A.; Sastre, G., From microscopic insights of H2 adsorption to uptake estimations in MOFs. *Physical Chemistry Chemical Physics* **2011,** *13* (37), 16558.
25. Couck, S.; Rémy, T.; Baron, G. V.; Gascon, J.; Kapteijn, F.; Denayer, J. F. M., A pulse chromatographic study of the adsorption properties of the amino-MIL-53 (Al) metal–organic framework. *Physical Chemistry Chemical Physics* **2010,** *12* (32), 9413.
26. Moosavi, S. M.; Boyd, P. G.; Sarkisov, L.; Smit, B., Improving the Mechanical Stability of Metal-Organic Frameworks Using Chemical Caryatids. *ACS Cent Sci* **2018,** *4* (7), 832-839.
27. Lal, G.; Derakhshandeh, M.; Akhtar, F.; Spasyuk, D. M.; Lin, J.-B.; Trifkovic, M.; Shimizu, G. K. H., Mechanical Properties of a Metal–Organic Framework formed by Covalent Cross-Linking of Metal–Organic Polyhedra. *Journal of the American Chemical Society* **2018,** *141* (2), 1045-1053.
28. Xie, X.-Y.; Wu, F.; Liu, X.; Tao, W.-Q.; Jiang, Y.; Liu, X.-Q.; Sun, L.-B., Photopolymerization of metal–organic polyhedra: an efficient approach to improve the hydrostability, dispersity, and processability. *Chemical Communications* **2019,** *55* (44), 6177-6180.
29. Hess, B.; Bekker, H.; Berendsen, H. J. C.; Fraaije, J. G. E. M., LINCS: A linear constraint solver for molecular simulations. *Journal of Computational Chemistry* **1997,** *18* (12), 1463-1472.
30. Darden, T.; York, D.; Pedersen, L., Particle Mesh Ewald - an N.Log(N) Method for Ewald Sums in Large Systems. *J. Chem. Phys.* **1993,** *98* (12), 10089-10092.
31. Bussi, G.; Donadio, D.; Parrinello, M., Canonical sampling through velocity rescaling. *J Chem Phys* **2007,** *126* (1), 014101.
32. Berendsen, H. J. C.; Postma, J. P. M.; Vangunsteren, W. F.; Dinola, A.; Haak, J. R., Molecular-Dynamics with Coupling to an External Bath. *Journal of Chemical Physics* **1984,** *81* (8), 3684-3690.
33. Ferey, G.; Mellot-Draznieks, C.; Serre, C.; Millange, F.; Dutour, J.; Surble, S.; Margiolaki, I., A chromium terephthalate-based solid with unusually large pore volumes and surface area. *Science* **2005,** *309* (5743), 2040-2.
34. Jorgensen, W. L.; Chandrasekhar, J.; Madura, J. D.; Impey, R. W.; Klein, M. L., Comparison of Simple Potential Functions for Simulating Liquid Water. *J. Chem. Phys.* **1983,** *79* (2), 926-935.
35. Jorgensen, W. L.; Tirado-Rives, J., The OPLS [optimized potentials for liquid simulations] potential functions for proteins, energy minimizations for crystals of cyclic peptides and crambin. *J Am Chem Soc* **1988,** *110* (6), 1657-66.
36. Abraham, M. J.; Murtola, T.; Schulz, R.; Páll, S.; Smith, J. C.; Hess, B.; Lindahl, E., GROMACS: High performance molecular simulations through multi-level parallelism from laptops to supercomputers. *SoftwareX* **2015,** *1-2*, 19-25.
37. Tribello, G. A.; Bonomi, M.; Branduardi, D.; Camilloni, C.; Bussi, G., PLUMED 2: New feathers for an old bird. *Computer Physics Communications* **2014,** *185* (2), 604-613.
38. Humphrey, W.; Dalke, A.; Schulten, K., VMD - Visual Molecular Dynamics. *Journal of Molecular Graphics* **1996,** *14*, 33-38.
39. Bonomi, M.; Bussi, G.; Camilloni, C.; Tribello, G. A.; Banáš, P.; Barducci, A.; Bernetti, M.; Bolhuis, P. G.; Bottaro, S.; Branduardi, D.; Capelli, R.; Carloni, P.; Ceriotti, M.; Cesari, A.; Chen, H.; Chen, W.; Colizzi, F.; De, S.; De La Pierre, M.; Donadio, D.; Drobot, V.; Ensing, B.; Ferguson, A. L.; Filizola, M.; Fraser, J. S.; Fu, H.; Gasparotto, P.; Gervasio, F. L.; Giberti, F.; Gil-Ley, A.; Giorgino, T.; Heller, G. T.; Hocky, G. M.; Iannuzzi, M.; Invernizzi, M.; Jelfs, K. E.; Jussupow, A.; Kirilin, E.; Laio, A.; Limongelli, V.; Lindorff-Larsen, K.; Löhr, T.; Marinelli, F.; Martin-Samos, L.; Masetti, M.; Meyer, R.; Michaelides, A.; Molteni, C.; Morishita, T.; Nava, M.; Paissoni, C.; Papaleo, E.; Parrinello, M.; Pfaendtner, J.; Piaggi, P.; Piccini, G.; Pietropaolo, A.; Pietrucci, F.; Pipolo, S.; Provasi, D.; Quigley, D.; Raiteri, P.; Raniolo, S.; Rydzewski, J.; Salvalaglio, M.; Sosso, G. C.; Spiwok, V.; Šponer, J.; Swenson, D. W. H.; Tiwary, P.; Valsson, O.; Vendruscolo, M.; Voth, G. A.; White, A.; The, P. c., Promoting transparency and reproducibility in enhanced molecular simulations. *Nature Methods* **2019,** *16* (8), 670-673.
40. Barducci, A.; Bussi, G.; Parrinello, M., Well-tempered metadynamics: a smoothly converging and tunable free-energy method. *Physical Review Letters* **2008,** *100* (2), 020603.
41. Gimondi, I.; Tribello, G. A.; Salvalaglio, M., Building maps in collective variable space. *J Chem Phys* **2018,** *149* (10), 104104.
42. Ryckaert, J.-P.; Bellemans, A., Molecular dynamics of liquid alkanes. *Faraday Discussions of the Chemical Society* **1978,** *66*, 95.
43. Tiwary, P.; Parrinello, M., A time-independent free energy estimator for metadynamics. *J Phys Chem B* **2015,** *119* (3), 736-42.
44. Caleman, C.; van Maaren, P. J.; Hong, M.; Hub, J. S.; Costa, L. T.; van der Spoel, D., Force Field Benchmark of Organic Liquids: Density, Enthalpy of Vaporization, Heat Capacities, Surface Tension, Isothermal Compressibility, Volumetric Expansion Coefficient, and Dielectric Constant. *Journal of Chemical Theory and Computation* **2012,** *8* (1), 61-74.

45. van der Spoel, D.; van Maaren, P. J.; Caleman, C., GROMACS molecule & liquid database. *Bioinformatics* **2012,** *28* (5), 752-753.

46. Schauperl, M.; Podewitz, M.; Waldner, B. J.; Liedl, K. R., Enthalpic and Entropic Contributions to Hydrophobicity. *Journal of Chemical Theory and Computation* **2016,** *12* (9), 4600-4610.

47. Gallo, P.; Corradini, D.; Rovere, M., Do ions affect the structure of water? The case of potassium halides. *Journal of Molecular Liquids* **2014,** *189*, 52-56.

Graphic entry for the Table of Contents (TOC)